

# Role of the glassy dynamics and thermal mixing in the dynamic nuclear polarization and relaxation mechanisms of pyruvic acid

M. Filibian<sup>1</sup>, S. Colombo Serra<sup>2</sup>, M. Moscardini<sup>1</sup>, A. Rosso<sup>3</sup>, F. Tedoldi<sup>2</sup> and P. Carretta<sup>1</sup>

<sup>1</sup> *University of Pavia, Department of Physics, Via Bassi 6, 27100-Pavia, Italy*

<sup>2</sup> *Centro Ricerche Bracco, Bracco Imaging Spa, via Ribes 5, 10010 Colletterto Giacosa (TO), Italy.*

<sup>3</sup> *Université Paris-Sud, CNRS, LPTMS, UMR 8626, Orsay F-91405, France.*

The temperature dependence of  $^1\text{H}$  and  $^{13}\text{C}$  nuclear spin-lattice relaxation rate  $1/T_1$  has been studied in the 1.6 K - 4.2 K temperature range in pure pyruvic acid and in pyruvic acid containing trityl radicals at a concentration of 15 mM. The temperature dependence of  $1/T_1$  is found to follow a quadratic power law for both nuclei in the two samples. Remarkably the same temperature dependence is displayed also by the electron spin-lattice relaxation rate  $1/T_{1e}$  in the sample containing radicals. These results are explained by considering the effect of the structural dynamics on the relaxation rates in pyruvic acid. Dynamic nuclear polarization experiments show that below 4 K the  $^{13}\text{C}$  build up rate scales with  $1/T_{1e}$ , in analogy to  $^{13}\text{C}$   $1/T_1$  and consistently with a thermal mixing scenario where all the electrons are collectively involved in the dynamic nuclear polarization process and the nuclear spin reservoir is in good thermal contact with the electron spin system.

## I. INTRODUCTION

In recent years Dynamic Nuclear Polarization (DNP) has been shown to be one of the most promising technique for hyperpolarizing nuclear spins. DNP increases the nuclear steady state polarization thanks to a transfer of magnetic order from the electron to the nuclear spins under microwave irradiation close to the electron Larmor frequency ( $\omega_e$ ). The application of DNP has catalyzed major advances in the Nuclear Magnetic Resonance (NMR) of low sensitivity nuclei in nanosized materials [1], in the high resolution NMR of biological samples [2, 3] and in *in vivo* real time imaging of biomolecules, hardly achievable with other methods [4]. For preclinical Magnetic Resonance Imaging (MRI) DNP is performed in solutions containing diamagnetic biomolecules labelled with  $^{13}\text{C}$  and a small concentration of stable radicals. The mixture is cooled down to about 1 K and, once the maximum  $^{13}\text{C}$  polarization is reached, it is rapidly dissolved [5–7] and injected *in vivo*, where the metabolic processes accessed by the hyperpolarized substrates are monitored by means of  $^{13}\text{C}$  MRI or Spectroscopy [4, 8, 9].

While significant scientific and technological efforts are nowadays spent to introduce dissolution DNP into the clinical practice [10–12], there is growing interest in the fundamental investigation of the physical mechanisms driving DNP. The first basic description of the DNP phenomenology dates to a few decades ago [13], when different regimes, the Solid Effect, the Cross Effect and the Thermal Mixing (TM), were defined depending on the magnitude of parameters such as the nuclear resonance frequency ( $\omega_L$ ), the coupling among the electron and nuclear spins and the external magnetic field strength. The most common and relevant regime for the molecules utilized in metabolic imaging is seemingly the TM [5, 7, 14], which is effective when the electron resonance linewidth is larger than  $\omega_L$  and the interactions among nuclear and electron spins are large enough to establish a common

spin temperature for the two reservoirs.

The TM regime is attained in pyruvic acid (PA) labelled with  $^{13}\text{C}$  and doped with a concentration of trityl radicals ( $c$ ) of the order of 10 mM [14–16]. PA has been up to date the most widely investigated system for *in vivo* DNP applications due to its role in glycolytic pathways [8, 9] and it can be considered as a prototype system to study the TM regime. Several DNP experiments have shown  $^{13}\text{C}$  polarizations approaching 20-30 % in PA doped with trityl radicals, at a temperature  $T \simeq 1.2$  K and for a magnetic field ( $H$ ) of 3.35 Tesla [5, 8]. In order both to optimize and to validate novel theoretical models of TM, several investigations of the nuclear and electron relaxation processes around 1.2 K have been performed. The effect of relevant parameters, including the radical concentration [14–16], the concentration of gadolinium complexes [14, 17], the nuclear concentration [18, 19], the amount of matrix deuteration [20], the effect of microwave saturation and the field strength [15, 16, 21] on the DNP performances of this molecule have been experimentally studied. Remarkably very recently, the relevance of these physical quantities on DNP kinetics has also been considered in the development of novel models describing TM throughout a rate equation approach [19, 22, 23]. Nevertheless, the role of the properties of the glassy matrix formed by the polarized molecules and radicals has not been investigated to a deep level.

The importance to achieve a glassy matrix, yielding a homogeneous distribution of internuclear and electron-nuclear distances in order to optimize DNP, has been well recognized [2, 18, 24] but a detailed study of the glassy dynamics of PA below 5 K and its effect on DNP has not been addressed up to date. In this regard the investigation of the spin dynamics of nuclei such as  $^1\text{H}$ , not involved in TM, can eventually help to identify the relaxation processes driven by the coupling with the glassy dynamics.

In this paper a  $^1\text{H}$  and  $^{13}\text{C}$  NMR study of pure PA and PA containing trityl radicals at a concentration of 15

mM is presented. It is shown that the spin-lattice relaxation rate ( $1/T_1$ ) of  $^1\text{H}$  and  $^{13}\text{C}$  nuclei and of the radical electron spins show all a nearly quadratic  $T$ -dependence below 4.2 K. Remarkably, while the  $^1\text{H}$  spin-lattice relaxation rate ( $1/T_{1\text{H}}$ ) is scarcely affected by the presence of paramagnetic radicals, the  $^{13}\text{C}$  spin-lattice relaxation rate ( $1/T_{1\text{C}}$ ) shows a sizeable enhancement upon paramagnetic doping. Moreover, the  $^{13}\text{C}$  polarization build up rate is found to follow the same  $T$  dependence of the spin-lattice relaxation rates. All these results are explained, below 4 K, in terms of the glassy dynamics which characterizes the PA and by resorting, for  $^{13}\text{C}$  DNP and spin-lattice relaxation, to the TM approach in the regime of good thermal contact between the nuclear and electron spin systems.

## II. EXPERIMENTAL METHODS AND TECHNICAL ASPECTS

$1\text{-}^{13}\text{C}$  pyruvic acid (PA) and un-labeled pyruvic acid (uPA) were purchased by Sigma Aldrich. The free radical trityl OX063 (tris(8-carboxyl-2,2,6,6-benzo(1,2-d:5-d)-bis(1,3)dithiole-4-yl)methyl sodium salt) was kindly provided by Albeda Research. For NMR and DNP experiments, 100  $\mu\text{L}$  of PA and of uPA, a 15 mM solution of OX063 in 100  $\mu\text{L}$  of  $1\text{-}^{13}\text{C}$  pyruvic acid (PA15) and a 15 mM solution of OX063 in 100  $\mu\text{L}$  of unlabelled pyruvic acid (uPA15) were transferred inside quartz tubes and sonicated for 10 minutes. The samples were cooled down to 4.2 K following several procedures, detailed in Appendix 6.1.

DNP experiments were performed by means of a homemade polarizer. A DNP-NMR probe was inserted in a bath cryostat and placed inside a superconducting magnet. Within that apparatus the temperature could be carefully controlled through helium adiabatic pumping between 1.6 K and 4.2 K. DNP was achieved by irradiating the samples with microwaves (MW) emitted by a Gunn-diode source operating in the 96-98 GHz frequency range, with a nominal output power of 30 mW.  $^1\text{H}$  and  $^{13}\text{C}$  NMR probe radiofrequency (RF) circuits were tuned at 37.02 MHz and accordingly the static magnetic field  $H$  was set to 0.87 Tesla and to 3.46 Tesla, respectively. The NMR signals were acquired with a solid-state Apollo Tecmag NMR spectrometer coupled to a homemade RF probe.  $^1\text{H}$  NMR spin-lattice relaxation time ( $T_{1\text{H}}$ ) was measured using standard saturation recovery sequences with a  $\pi/2$  pulse length in the 2 – 3  $\mu\text{s}$  range. In all samples  $^1\text{H}$  recovery law was described by  $y(\tau) = M_0[1 - \exp(-\tau/T_{1\text{H}})]$  (Fig. 1), indicating that all the protons are characterized by a common spin temperature.  $^1\text{H}$  and  $^{13}\text{C}$  NMR spin-spin relaxation times ( $T_{2\text{H}}$  and  $T_{2\text{C}}$ ) were measured by means of the Hahn Echo sequence.

DNP experiments were performed by irradiating the sample at the MW frequency maximizing the positive polarization enhancement, about 97 GHz at 3.46 Tesla. In

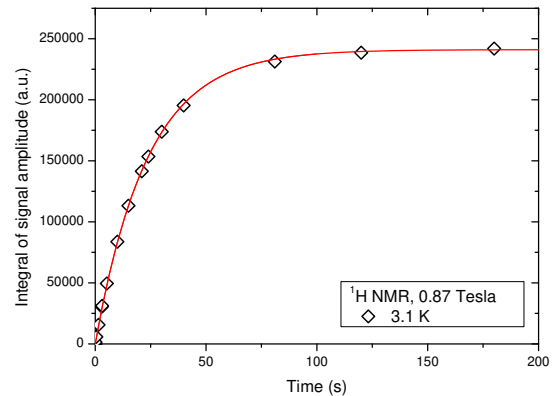


FIG. 1: Recovery law for  $^1\text{H}$  nuclear magnetization in PA at 3.1 K and 0.87 Tesla after a saturating pulse sequence. The solid red line is the best fit according to the function  $y(\tau) = M_0(1 - \exp(-\tau/T_{1\text{H}}))$ .

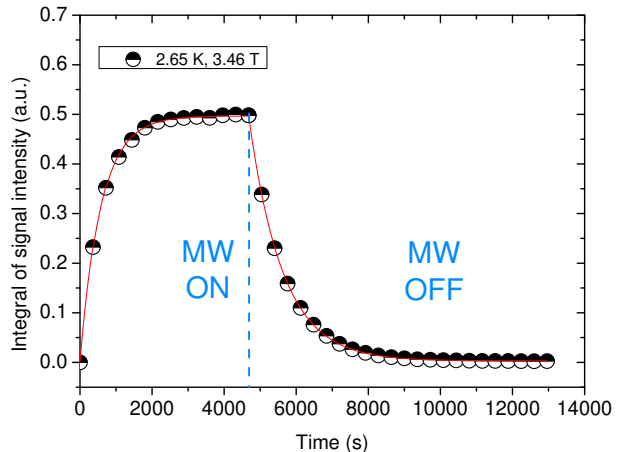


FIG. 2:  $^{13}\text{C}$  polarization build-up under MW irradiation (MW ON) and relaxation to the thermal equilibrium value of the nuclear magnetization (MW OFF) in PA15 at 2.67 K and 3.46 T. The red lines are fits according to the functions explained in the text.

order to acquire  $^{13}\text{C}$  build up curves, the  $^{13}\text{C}$  NMR signal was sampled under MW irradiation after RF saturation (Fig. 2). The Free Induction Decay (FID) signal was acquired up to steady state applying subsequent low flip angle readout pulses (about  $6^\circ$ ) [5] with a repetition time  $\tau$  between 120 s and 600 s.  $^{13}\text{C}$  steady state polarization  $P_{\infty}$  and the polarization time constant  $T_{\text{pol}}$ , describing the progressive growth of the polarization, were derived by fitting the build up curves to an expression that takes into account the reduction of the  $^{13}\text{C}$  signal amplitude

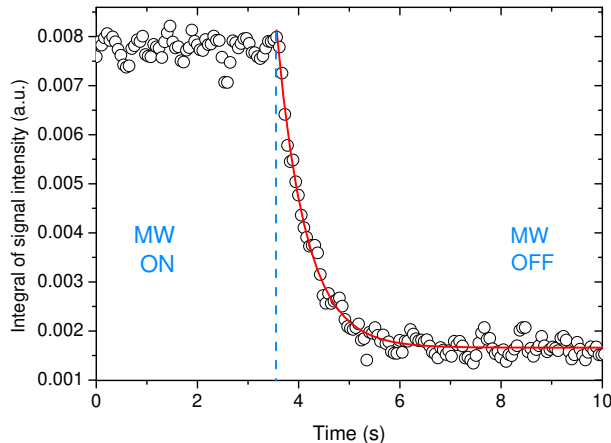


FIG. 3: Integral of the imaginary part of the  $^{13}\text{C}$  signal as a function of time in PA15 at 2 K by means of a low flip angle acquisition scheme with  $\alpha = 3^\circ$  and  $\tau = 30$  ms. In this experiment the MW were switched off 3.5 s after the sequence start. Data have been corrected by the artificial decay induced by the application of the readout pulses. The points collected after switching off MW could be fit to a simple exponential decay  $y(t) = A \exp(-t/T_{1e})$  (red curve).

induced by the readout pulses [25]. In the absence of MW irradiation the same sequence was used to measure  $^{13}\text{C}$   $T_1$  ( $T_{1C}$ ) by following the build up of the  $^{13}\text{C}$  NMR signal to the thermal equilibrium value after RF saturation. Alternatively,  $T_{1C}$  was derived from the decay of the steady state polarization to thermal equilibrium after switching off the MW, again measured by using a low flip angle (about  $6^\circ$ ) sequence (Fig. 2). The  $^{13}\text{C}$  NMR signal decay was fit to the following expression

$$M(t) = M_\infty \exp \left[ - \left( \frac{t}{T_{1C}} - \frac{t \ln(\cos \alpha)}{\tau} \right) \right] + M_0, \quad (1)$$

with  $M_\infty$  the steady state  $^{13}\text{C}$  magnetization under MW irradiation,  $\alpha$  the flip angle,  $\tau$  the repetition time (300 s - 800 s) and  $M_0$  the  $^{13}\text{C}$  thermal equilibrium magnetization. The logarithmic term in Eq. 1 takes into account the artificial reduction of the NMR signal induced by the readout pulses.

The electron spin-lattice relaxation time  $T_{1e}$  was derived indirectly by observing the effect of the time evolution of electron spin polarization on the NMR paramagnetic shift, and hence on the NMR signal, after the MW were turned off. In particular, after RF saturation the sample was polarized under MW irradiation for about 10-15 minutes. This time is enough for the electrons to reach steady state saturation and, additionally, to increase the  $^{13}\text{C}$  signal-to-noise ratio significantly without having to wait the long time required to reach  $P_{N\infty}$ . Subsequently, a low flip angle acquisition sequence was started, with  $3^\circ$  flip angles and with time delay between consecutive FID acquisitions between 15 ms and 100 ms. Around 3-9 s

after the beginning of the sequence, MW were switched off and the  $^{13}\text{C}$  NMR signal was followed for few seconds. During this time window, since the nuclear relaxation is orders of magnitude slower than the electronic one, the paramagnetic shift of the  $^{13}\text{C}$  NMR line  $\Delta\omega_0$  is found to vary proportionally to  $P_e(t) \propto \exp(-t/T_{1e})$  and to finally reach a plateau. The variation of  $\Delta\omega_0$  correspondingly implies a modification of the shape of the NMR signal. Jóhannesson et al. [15] have described a detailed procedure which allows to analyze the NMR signal shape and to quantify the  $^{13}\text{C}$  NMR line shift. However as long as the precise determination of the line shift is not concerned, more workable approaches can be adopted to estimate  $T_{1e}$ . In this work  $T_{1e}$  was extracted by fitting the decay of the integral of the imaginary part of the  $^{13}\text{C}$  signal  $I(t)$ , obtained after switching MW off, to a simple exponential decay  $A \exp(-t/T_{1e})$  (Fig. 3). Further details on the procedure used to derive  $T_{1e}$  are given in Appendix 6.2, where a complete description of the NMR shift time dependence in presence of both electron polarization dynamics and the nuclear polarization dynamics is also provided and discussed.

### III. EXPERIMENTAL RESULTS

A different behaviour of  $1/T_{1H}$  and  $1/T_{1C}$  data was observed by changing the cooling rate of PA and PA15 below 300 K. The cooling rate dependence of  $1/T_{1C}$  and the cooling procedures are described in detail in Appendix 6.1. All the relaxation measurements presented in the following were performed after flash freezing the samples in liquid helium. The  $T$  dependence of  $1/T_{1H}$  and  $1/T_{1C}$ , derived as explained in Section 2, are shown in Figs. 4, 5 and 6. The data in Fig. 4 and 5, measured in PA, PA15 and uPA15 by keeping the same  $\omega_L$  for the two nuclei, evidence that both  $1/T_{1H}(T)$  and  $1/T_{1C}(T)$  roughly follow a similar power law  $\sim T^2$  (Table I). It is further remarked that in PA15 the prolongation of the fit curve of  $1/T_{1C}(T)$  down to 1.15 K (Fig. 5) closely approaches the value reported for an analogous sample in Ref. [14].

In Fig. 6 the comparison between  $1/T_{1H}(T)$  obtained in uPA15 and uPA is depicted. One can observe that also in the radical free uPA sample  $1/T_{1H}(T)$  follows a  $\sim T^2$  power law and, moreover, the comparison between the two samples enlightens that the addition of 15 mM of OX063 radicals yields only a minor enhancement of  $1/T_{1H}(T)$  in the explored  $T$  range ( $T_{1H}(\text{uPA15})/T_{1H}(\text{uPA}) \simeq 1.2 \div 1.3$ ). It is noticed that  $1/T_{1H}(T)$  increases by a slightly lower amount of +15% in the PA sample, in which also  $1\text{-}^{13}\text{C}$  nuclei are present.

For the spin-spin relaxation times, we estimated an almost  $T$ -independent  $T_{2C} \approx 190 \mu\text{s}$  and  $T_{2H} \approx 35 \mu\text{s}$  in PA below 4.2 K. Also the width of the NMR line was constant over the same  $T$  range. The  $^1\text{H}$  lines of both PA and PA15 were fit to a Gaussian with a nearly equal Full Width at Half Maximum (FWHM) of  $30.0 \pm 0.4$  kHz in PA and of  $31.4 \pm 0.6$  kHz in PA15 between 1.6 K and

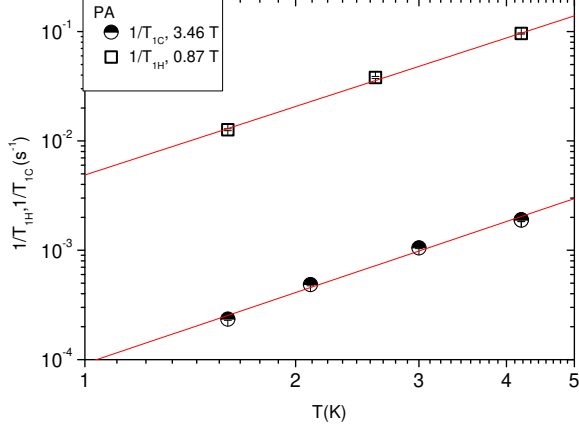


FIG. 4: Log-log plot of  $1/T_{1H}(T)$  (squares) and  $1/T_{1C}(T)$  (circles) in PA below 4.2 K. The red lines are fits to the power law  $y(T) = aT^b$ , yielding  $a = 9.19 \pm 1.1 \cdot 10^{-5}$  and  $b = 2.16 \pm 0.11$  for  $1/T_{1C}(T)$  and  $a = 4.88 \pm 0.44 \cdot 10^{-3}$  and  $b = 2.08 \pm 0.07$  for  $1/T_{1H}(T)$ .

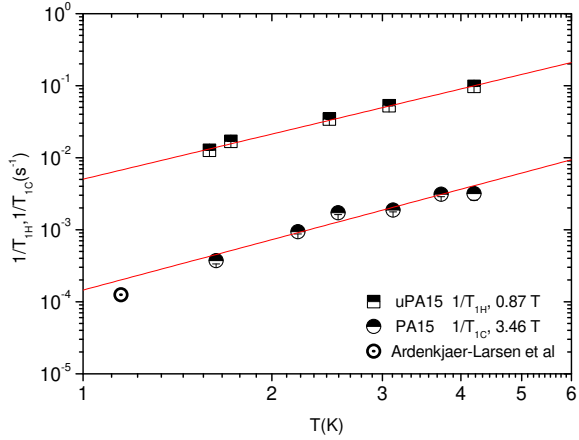


FIG. 5: Log-log plot of  $1/T_{1H}(T)$  (squares) in uPA15 and of  $1/T_{1C}(T)$  in PA15 (circles) below 4.2 K. The red lines are fits to the power law  $y(T) = aT^b$ , yielding  $a = 1.45 \pm 0.46 \cdot 10^{-4}$  and  $b = 2.32 \pm 0.3$  for  $1/T_{1C}(T)$  and  $a = 5.03 \pm 0.29 \cdot 10^{-3}$  and  $b = 2.08 \pm 0.06$  for  $1/T_{1H}(T)$ .

4.2 K (Fig. 7). Differently,  $^{13}\text{C}$  lines displayed a Voigtian lineshape with a FWHM of  $5.9 \pm 0.1$  kHz in PA and of  $6.1 \pm 0.1$  kHz in PA15 (Fig. 7). The additional 200 Hz broadening in PA15 could be due to the coupling with electrons, however it is also of the order of the possible broadening due to the field inhomogeneity.

Remarkably, also the electron spin-lattice relaxation rate  $1/T_{1e}(T)$  measured after a flash freezing procedure (Fig. 8) could be fit to a  $\sim T^2$  power law (Table I). It can be noticed that  $T_{1e}$  increases progressively upon cooling

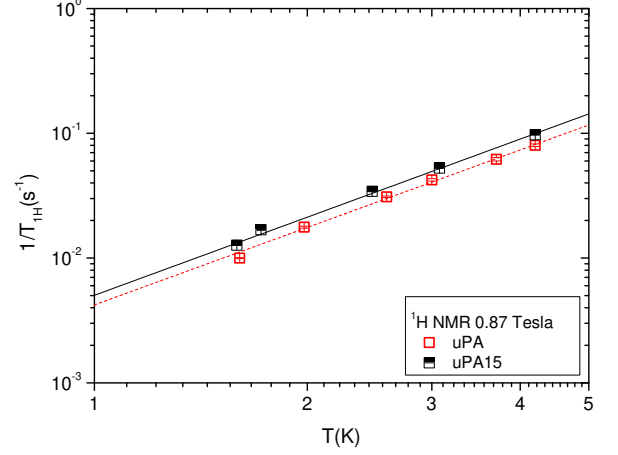


FIG. 6: Log-log plot of  $1/T_{1H}(T)$  measured in uPA15 (black squares) and in uPA (red squares) below 4.2 K. Both the black and the red lines are fits to the power law  $y(T) = aT^b$ . The black line is the same data fit of  $1/T_{1H}(T)$  in PA15 reported in Fig. 5, while the red line has been obtained with the parameters  $a = 4.21 \pm 0.31 \cdot 10^{-3}$  and  $b = 2.06 \pm 0.06$ .

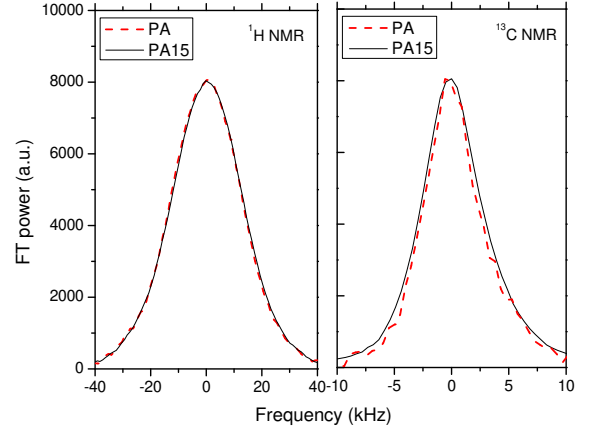


FIG. 7: A comparison between the NMR lines of  $^1\text{H}$  in PA and PA15 (Left) and of  $^{13}\text{C}$  in PA and in PA15 (right) measured around 1.8 K. The frequencies in kHz are reported as shifts from the spectrometer frequency of 37.02 MHz. In order to compare the different NMR lines, all the plots have been centred around this same reference frequency.

until it reaches 1.5 s around 1.6 K, a value close to the one reported in the literature at  $T = 1.2$  K [14].

Now the  $T$  dependence of the two characteristic DNP parameters  $T_{\text{pol}}$  and  $P_{N\infty}$  for the PA15 sample is presented. As shown in Fig. 9,  $1/T_{\text{pol}} \sim 1/T_{1C} \approx 3 \div 4 \cdot 10^{-3} \text{ s}^{-1}$  around 4.2 K and reduces significantly on cooling. Correspondingly  $T_{\text{pol}}$  reaches values around 1500 s for  $T \simeq 1.6$  K, much shorter than  $T_{1C} \simeq 3000$  s at the same

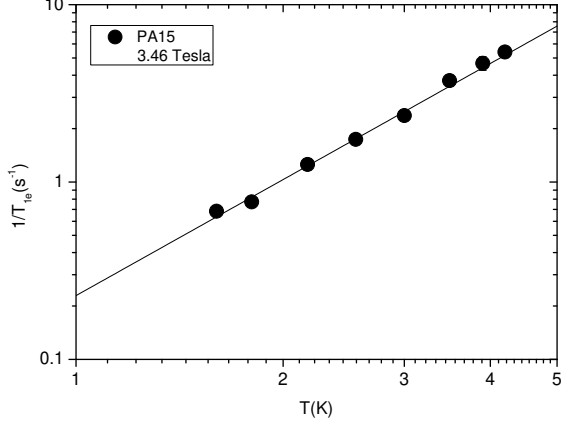


FIG. 8: Log-log plot of  $1/T_{1e}(T)$  in PA15 below 4.2 K. The black lines is a fit to the power law  $y(T) = aT^b$ , yielding  $a = 0.23 \pm 0.01 \cdot 10^{-5}$  and  $b = 2.17 \pm 0.07$ .

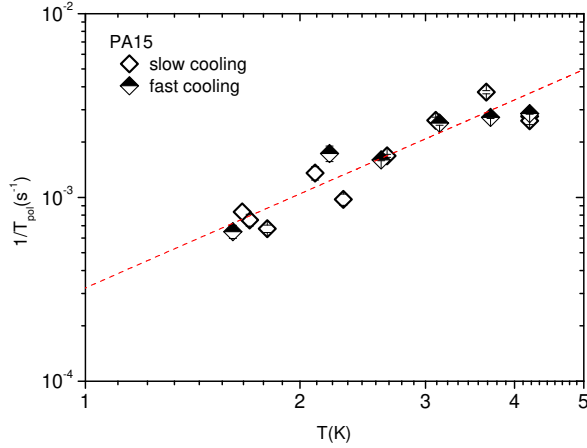


FIG. 9: Log-log plot of  $1/T_{pol}(T)$  in PA15 below 4.2 K measured after a slow cooling (white diamonds) and a fast cooling (black and white diamonds) procedure. The dashed line is a fit according to the power law  $y(T) = aT^b$ , yielding  $a = 3.02 \pm 0.27 \times 10^{-4}$  and  $b = 1.70 \pm 0.18$ .

$T$ . Moreover,  $T_{pol}$  values at the lowest  $T$  of 1.6 K are close to the ones reported in the literature at  $T \simeq 1.2$  K [16]. Also  $1/T_{pol}$  follows a power law  $aT^b$  with  $b \simeq 1.7$  (Table I) in substantial agreement with literature papers suggesting a proportionality between  $T_{pol}(T)$  and  $T_{1e}(T)$  [26, 27] and reporting a divergence of  $T_{1C}$  and  $T_{pol}$  (Fig.11) at very low  $T$  [5, 14, 15, 18, 26–31]. Never-

theless, to our knowledge the mechanism responsible for this phenomenon has not been specifically addressed to date.

The values of the steady state polarization  $P_{N\infty}$  for the PA15 sample, derived from the build up curves between 1.6 K and 4.2 K are reported in Fig. 10 as a function of  $1/T$ .  $P_{N\infty}$  reaches already a sizeable value, around 3-4 %, at 4.2 K which raises up to 15.5 % at 1.6 K, with a linear trend at high  $T$  that turns into a non linear bend at lower  $T$  (for  $1/T > 0.4 \text{ K}^{-1}$ , i.e.  $T < 2.5 \text{ K}$ ). These values of  $P_{N\infty}$ , as well as the presence of the bending, cannot be explained in the framework of the traditional Borghini model [13, 32] which predicts a polarization of  $\sim 80\%$  at low  $T$  and an opposite curvature for the bending. Finally it is noted that, unlike nuclear spin-lattice relaxation data, both  $T_{pol}$  and  $P_{N\infty}$  do not depend on the cooling rate.

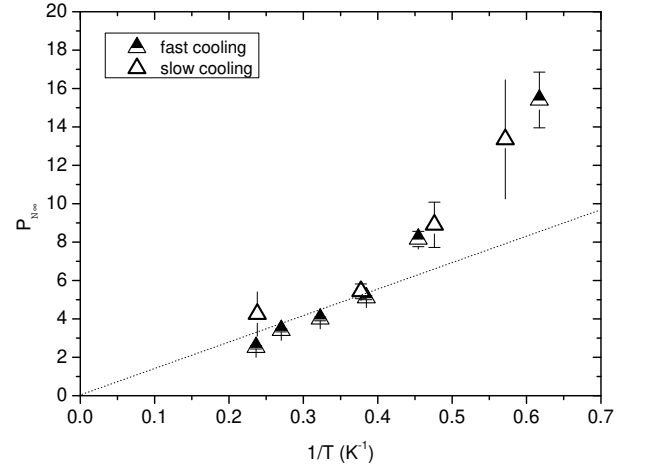


FIG. 10:  $P_{N\infty}$  as a function of  $T$  in PA15 measured after a slow cooling (white triangles) and a fast cooling (black and white triangles) procedure. The error bars with caps have been estimated by the best fit of polarization buildup curves, while the error bars without caps indicate the standard deviation for a series of repeated measurements.

TABLE I: Fit results of the NMR and DNP measurements according to the law  $y(T) = aT^b$  in PA samples at 3.46 Tesla

Sample	Measurement	$a \text{ (s}^{-1} \cdot \text{K}^{-b})$	$b$
PA	$1/T_{1C}(T)$	$9.19 \pm 1.11 \times 10^{-5}$	$2.16 \pm 0.11$
PA	$1/T_{1H}(T)$	$4.88 \pm 0.44 \times 10^{-3}$	$2.08 \pm 0.07$
uPA	$1/T_{1H}(T)$	$4.21 \pm 0.31 \times 10^{-3}$	$2.06 \pm 0.06$
PA15	$1/T_{1C}(T)$	$1.45 \pm 0.46 \times 10^{-4}$	$2.32 \pm 0.3$
uPA15	$1/T_{1H}(T)$	$5.03 \pm 0.29 \times 10^{-3}$	$2.08 \pm 0.06$
PA15	$1/T_{1e}(T)$	$0.23 \pm 0.01$	$2.17 \pm 0.07$
PA15	$1/T_{pol}(T)$	$3.02 \pm 0.27 \times 10^{-4}$	$1.70 \pm 0.18$



## IV. DISCUSSION

### A. Nuclear spin-lattice relaxation in pyruvic acid

First we shall start considering the different contributions to nuclear spin-lattice relaxation rate in PA. The main contribution to  $1/T_{1H}$  arises from the dipolar  $^1\text{H}$ - $^1\text{H}$  coupling while only a minor contribution ( $< 15\%$ ) due to  $^1\text{H}$ - $^{13}\text{C}$  interaction is present, as it is evidenced by comparing  $1/T_{1H}$  in PA and uPA samples. Thus in PA  $1/T_{1H}$  can be expressed as the sum of independent terms

$$\left(\frac{1}{T_{1H}}\right)_{PA} = \left(\frac{1}{T_1}\right)_{^1H-^1H} + \left(\frac{1}{T_1}\right)_{^{13}C-^1H}, \quad (2)$$

where  $(1/T_1)_{^1H-^1H}$  sums up the contributions from intra and intermolecular proton-proton dipolar interactions and  $(1/T_1)_{^{13}C-^1H}$  originates from carbon-proton intramolecular interactions. Accordingly, in uPA the second term must be omitted. Similarly, in PA the  $^1\text{H}$  line broadening can be ascribed mostly to  $^1\text{H}$ - $^1\text{H}$  interactions. In fact, it is nearly 30 kHz in both PA and uPA, which demonstrates that the line broadening due to the  $^1\text{H}$ - $^{13}\text{C}$  interaction in the COOH group is much smaller than the  $^1\text{H}$ - $^1\text{H}$  coupling. Upon neglecting the  $^1\text{H}$ - $^{13}\text{C}$  interaction, from the second moment of the proton line one can definitely estimate a mean square amplitude of the dipolar field probed by protons  $\sqrt{\langle \Delta h^2 \rangle} \simeq 7.6 \cdot 10^{-4}$  Tesla.

For  $^{13}\text{C}$  the relevant intra and intermolecular heteronuclear dipolar interactions take place between the carboxyl  $^{13}\text{C}$  and the methyl and hydroxyl protons. This coupling significantly overcomes the homonuclear  $^{13}\text{C}$ - $^{13}\text{C}$  one. In fact, as it is described in detail in Appendix 6.3, according to the  $1/T_1$  expression for homonuclear (Eq. 16) and heteronuclear (Eq. 17) interactions, the ratio

$$\frac{(T_1)_{^1H-^{13}C}}{(T_1)_{^{13}C-^{13}C}} \simeq 3 \left(\frac{\gamma_C}{\gamma_H}\right)^2 \frac{\langle \frac{1}{r_{CC}^6} \rangle}{\langle \frac{1}{r_{HC}^6} \rangle} \sim 10^{-4}, \quad (3)$$

where  $\gamma_C$  is the  $^{13}\text{C}$  gyromagnetic ratio and  $\gamma_H$  the  $^1\text{H}$  gyromagnetic ratio,  $\langle 1/r_{HC}^6 \rangle$  indicates the average of the inverse sixth power of  $^1\text{H}$ - $^{13}\text{C}$  distances  $r_{HC}$  and  $\langle 1/r_{CC}^6 \rangle$  is the same quantity referred to  $^{13}\text{C}$ - $^{13}\text{C}$  distances  $r_{CC}$ . This difference is simply due to the fact that the average intermolecular  $r_{CC}$  is significantly larger than the intramolecular  $r_{HC}$ <sup>1</sup>. Additionally, in the case of  $1/T_{1C}$  a further mechanism, involving the fluctuations of the chemical shift tensor (CSA), should be considered and thus, neglecting the weak homonuclear interactions, for

PA one can write

$$\left(\frac{1}{T_{1C}}\right)_{PA} = \left(\frac{1}{T_1}\right)_{^1H-^{13}C} + \left(\frac{1}{T_1}\right)_{\text{CSA}}, \quad (4)$$

where  $(1/T_1)_{\text{CSA}}$  refers to the fluctuations of the CS tensor. Accordingly, the  $^{13}\text{C}$  linewidth (5.9 kHz) cannot be explained by considering the  $^1\text{H}$ - $^{13}\text{C}$  dipolar coupling only. In this respect Macholl et al.[16] report a calculation of the  $^{13}\text{C}$  CS tensor parameters in PA, that retrieved the shielding anisotropy  $\Delta\sigma \simeq 130$  ppm and is thus responsible of a broadening at half height of the  $^{13}\text{C}$  line of  $\Delta\sigma\omega_C = 4.8$  kHz at  $H=3.35$  T and the Larmor frequency  $\omega_C = \gamma_C H$ . Only the remaining broadening, at most 3.4 kHz, should thus be ascribed to  $^1\text{H}$ - $^{13}\text{C}$  couplings. This explains also why  $^1\text{H}$ - $^{13}\text{C}$  yields a negligible contribution to the  $^1\text{H}$  linewidth (less than 10 % of the total width).

Now it is interesting to compare the ratio  $T_{1C}(T)/T_{1H}(T) \simeq 53$  (Fig. 4) derived experimentally for the Larmor frequency  $\omega_H/2\pi = (\gamma_H/2\pi)H_1$  equal to  $\omega_C/2\pi = (\gamma_C/2\pi)H_2 = 37.02$  MHz ( $H_1 = 0.87$  Tesla and  $H_2 = 3.46$  Tesla), with the one that can be estimated theoretically by considering the different contributions to the nuclear spin-lattice relaxation. One can start calculating that ratio under the assumption that the spectral density  $J(\omega)$  is the same for all the relaxation contributions and specializing their expression taking into account both the dipolar and CSA relaxation mechanisms (see Eq.16 and 17 in Appendix 6.3). Under that assumption one finds an extremely good agreement between the calculated  $T_{1C}(T)/T_{1H}(T) \simeq 54$  (see Appendix 6.3) and the experimental value, which indicates that the  $1/T_1$  models in Eq. 2 for  $^1\text{H}$  and in Eq. 4 for  $^{13}\text{C}$  are likely correct. The fact that the same  $J(\omega)$  describes the relaxation mechanisms for the two nuclear species in PA will be further discussed in the following Subsection.

### B. The role of the glassy matrix in the relaxation rates

The nature of the excitations leading to the spin-lattice relaxation is now analyzed. The common  $T^2$  dependence of  $1/T_{1H}(T)$ ,  $1/T_{1C}(T)$  and  $1/T_{1e}(T)$  strikingly points to the presence of a common source of relaxation. In particular, while the nuclear spin-lattice relaxation is dominated by the fluctuations of the dipolar interactions with the other nuclei and with the electrons in PA15 (discussed in Subsection 4.3), the electron spin-lattice relaxation of the diluted radicals is rather induced by scattering with the vibrational modes. Therefore, the lattice vibrations seem to be responsible both for spatial modulation of dipolar couplings at the nuclear Larmor frequency and for the excitation of electron spin transitions at the electron Larmor frequency. The existence of a such a broad spectral density of lattice excitations, even at liquid helium T, should not surprise, since solid PA is an organic

<sup>1</sup> The shortest  $r_{HC}$  found in the COOH group is about 1.84 Å in the most abundant pyruvic acid conformer [33] while the intermolecular  $r_{CC}$  should rather be closer to 5.5 Å, equal to twice the Van Der Waals radius of the PA molecule.

glass [34, 35]. Several physical properties of glasses can be described by assuming a local lattice dynamics, namely molecules or atoms can fluctuate among different configurations having very similar energy minima, separated by a barrier  $\Delta E$ . Upon increasing  $T$  the correlation time of these fluctuations can be described by an activated law  $\tau_c(T) = \tau_0 \exp(\Delta E/T)$ , with  $\tau_0$  the correlation time in the infinite  $T$  limit.

For each activation barrier,  $1/T_1$  can be simply described resorting to a spectral density of the form

$$\frac{1}{T_1} = \frac{\gamma^2 \langle \Delta h_{\perp}^2 \rangle}{2} J(\omega_L) = \frac{\gamma^2 \langle \Delta h_{\perp}^2 \rangle}{2} \frac{2\tau_c}{1 + \omega_L^2 \tau_c^2}, \quad (5)$$

where  $\langle \Delta h_{\perp}^2 \rangle$  is the mean square amplitude of the random fluctuating fields probed by the nuclei in the plane perpendicular to the magnetic field. By considering different types of distribution functions  $p(\Delta E)$  for the energy barriers one typically finds a low- $T$  power-law behaviour with  $1/T_1 \sim T^{1+\alpha}$  ( $0 \leq \alpha \leq 1$ ). A quadratic trend, as the one experimentally observed here, is obtained for  $p(\Delta E) \propto \Delta E$ . Notably, the same result was derived also taking into account the thermally activated dynamics in asymmetric double wells characterizing the glasses [36, 37] and a recent implementation of the same approach could explain also the quadratic  $T$  dependence of  $1/T_{1e}$  observed at low  $T$  in various amorphous materials, including organic glasses [38].

It is remarked that the magnetic field dependence of  $1/T_{1C}$  at 4.2 K shows that  $1/T_{1C} \propto 1/\omega_L^2$ , suggesting (see Eq.5) that basically all the lattice modes are characterized by low-frequency fluctuations such that  $\omega_L \tau_c \gg 1$ . This observation is also corroborated by the observation that  $^{13}\text{C}$  NMR linewidth is  $T$ -independent in the explored  $T$ -range, indicating that  $2\pi\Delta\nu\tau_c \gg 1$ . In the presence of such slow dynamics one can consider the slow motions limit of Eq.5, yielding  $1/T_1(T) \propto \langle 1/\tau_c(T) \rangle$ , where  $\langle 1/\tau_c \rangle$  represents an average correlation frequency of the fluctuations over the distribution  $p(\Delta E)$ .  $\langle 1/\tau_c(T) \rangle$  in uPA can be estimated by specializing  $\langle \Delta h_{\perp}^2 \rangle$  in Eq. 8 to the case of  $1/T_1$  driven by the dipolar interaction with like spins (Eq 16), obtaining [39]

$$\left( \frac{1}{T_{1H}} \right)_{uPA} = \frac{2}{5} \left( \frac{\mu_0}{4\pi} \right)^2 \frac{\gamma_H^4 \hbar^2 I(I+1)}{\omega_H^2} \left\langle \frac{1}{r_{HH}^6} \right\rangle \left\langle \frac{2}{\tau_c} \right\rangle, \quad (6)$$

where  $I = 1/2$  is the proton spin,  $r_{HH}$  the inter-proton distance and  $\omega_H/2\pi = 37.02$  MHz. Since the temperature dependence of  $1/T_1$  is entirely contained in  $\langle 1/\tau_c(T) \rangle$ , then  $\langle 1/\tau_c(T) \rangle = 1/T_1(T)1/C = A_1 * T^{B_1} * 1/C = AT^B$ , where  $C$  is a factor including the temperature independent parameters in Eq .6 and  $A_1$  and  $B_1$  are the fit parameters of  $1/T_1$  in uPA reported in Table 1. Then  $A = A_1/C$  and  $B = B_1$  and considering a mean dipolar field of  $7.6 \cdot 10^{-4}$  Tesla, as estimated from  $^1\text{H}$  NMR linewidth, one finds  $A \simeq 6.7 \times 10^3 \text{ s}^{-1} \cdot \text{K}^{-B}$  and  $B \simeq 2.06$ . The same procedure can be applied also to evaluate  $\langle 1/\tau_c(T) \rangle$  from  $^{13}\text{C}$  data in PA, by considering

Eq. 4, and Eq. 17, Eq. 18 in the slow motion regime (see also Appendix 6.3 and [39, 40])

$$\left( \frac{1}{T_{1C}} \right)_{PA} = \frac{2}{15} \left( \frac{\mu_0}{4\pi} \right)^2 \frac{754}{225} \gamma_C^2 \gamma_H^2 \hbar^2 I(I+1) \left\langle \frac{1}{r_{HC}^6} \right\rangle \frac{1}{\omega_C^2} \left\langle \frac{1}{\tau_c} \right\rangle + \frac{2}{15} \Delta\sigma^2 \left\langle \frac{1}{\tau_c} \right\rangle, \quad (7)$$

where  $\omega_C/2\pi = 37.02$  MHz. Using the value of  $\langle \Delta\omega_{\perp\text{CH}}^2 \rangle = 2/15(\mu_0/4\pi)^2 \gamma_C^2 \gamma_H^2 \hbar^2 I(I+1) \langle 1/r_{HC}^6 \rangle = 232.5 \text{ (krad/s)}^2$  obtained from the  $^{13}\text{C}$  linewidth analysis reported in literature, one finds  $A \simeq 5.5 \times 10^3 \text{ s}^{-1} \cdot \text{K}^{-B}$  and  $B \simeq 2.16$ , a value very close to the one calculated for protons. Again, this results do confirm that the leading modulation source for all the interactions probed by nuclei, both dipolar and due to CSA, is the glassy dynamics of the PA matrix.

### C. Nuclear spin-lattice relaxation in the presence of radicals

Upon doping PA with trityl radicals, the  $1/T_1$  analysis has to be modified in order to include also a relaxation term due to the coupling with the radical electron spins. Hence in PA15 Eqs. 2 and 4 are modified as

$$\left( \frac{1}{T_{1H}} \right)_{PA15} = \left( \frac{1}{T_1} \right)_{1H-1H} + \left( \frac{1}{T_1} \right)_{13C-1H} + \left( \frac{1}{T_{1H}} \right)_{el} \quad (8)$$

and

$$\left( \frac{1}{T_{1C}} \right)_{PA15} = \left( \frac{1}{T_1} \right)_{1H-13C} + \left( \frac{1}{T_1} \right)_{CSA} + \left( \frac{1}{T_{1C}} \right)_{el}, \quad (9)$$

where  $(1/T_1)_{el}$  is the contribution due to the hyperfine coupling between the nuclei and the radical electron spins. As it is evident from Fig. 6, the most relevant contributions to  $1/T_{1H}$  in PA15 is still due to the nucleus-nucleus dipolar interaction. Doping yields only a slight increment of  $1/T_{1H}$  in PA15 with respect to PA, of the order of  $+20 \div 30\%$ . On the other hand, according to Table I, one observes that  $T_{1C}(PA)/T_{1C}(PA15) \simeq 1.6$ , meaning that the electron contribution to  $T_{1C}$  is about  $2 \div 3$  times the one to  $T_{1H}$ .

Within a simplified model one could start analyzing these results by simply considering an electron contribution to the longitudinal relaxation of the  $^{13}\text{C}$  nuclei driven by the lattice dynamics only. As illustrated in Appendix 6.3, the average ratio  $T_{1C}(T)/T_{1H}(T) \simeq 28 \pm 3$  in PA15 (Fig. 5) can be reasonably explained within this framework. However, this simplified model suffers from several limitations being based on certain approximations for the magnitude of the fluctuating fields and of  $\tau_c$ . For example, it does not take into account the effect of spin diffusion. On the other hand, as it will be shown in Sect. 4.4,  $(1/T_{1C})_{el}$  can be quantitatively explained

without adjustable parameters in the framework of the TM approach.

Still,  $(1/T_{1H})_{el}$  cannot be ascribed to TM, because  $^1H$  nuclei are characterized by  $\omega_L$  larger than the electron spin resonance (ESR) linewidth. Thus, in the case of  $^1H$  nuclei,  $(1/T_{1H})_{el}$  should be due exclusively to the modulation of the electron dipolar field at the nucleus caused by the glassy dynamics. Accordingly one can estimate  $\langle 1/\tau_c(T) \rangle$  associated with  $1/T_{1H}$  due to radicals, given by  $(1/T_{1H})_{el} = (1/T_{1H})_{uPA15} - (1/T_{1H})_{uPA}$ , by applying the same approach adopted in the previous Subsection 4.2 and taking into account the appropriate magnitude of the hyperfine coupling. In particular, in the slow motion regime one can write [39]

$$\left( \frac{1}{T_{1H}} \right)_{el} = \frac{2}{5} \left( \frac{\mu_0}{4\pi} \right)^2 \frac{\gamma_e^2 \gamma_H^2 \hbar^2 S(S+1)}{\omega_H^2} \left\langle \frac{1}{r_{eH}^6} \right\rangle \left\langle \frac{1}{\tau_c} \right\rangle, \quad (10)$$

where  $S$  is the electron spin,  $\gamma_e$  the electron gyromagnetic ratio and  $r_{eH}$  the electron-proton distance. By assuming an average hyperfine field of  $\sqrt{\langle \Delta h_{eH}^2 \rangle} = 8.2 \cdot 10^{-4}$  Tesla at the  $^1H$  site<sup>2</sup>, very close to the one produced by the other nearby protons, one finds  $\langle 1/\tau_c(T) \rangle \simeq AT^B$  with  $A \simeq 2.3 \times 10^3 \text{ s}^{-1} \cdot \text{K}^{-B}$  and  $B \simeq 2.16$ . Remarkably, the  $\langle 1/\tau_c(T) \rangle$  describing the fluctuations leading to the relaxation term  $(1/T_{1H})_{el}$  is close to the one describing the glassy dynamics probed by  $(1/T_{1H})_{PA}$ . Then one can conclude that in presence of radicals the  $^1H$  relaxation involves the modulation of the field generated by the paramagnetic radicals, driven by the lattice glassy dynamics. Relaxation processes for  $(1/T_{1H})_{el}$  driven by electron spin flips can be disregarded since they should be characterized by a fluctuation frequency  $1/T_{1e}$  much smaller than the one of the glassy dynamics.

#### D. The effect of Thermal Mixing in $^{13}C$ spin-lattice relaxation and the electron spin-lattice relaxation

As it was pointed out in the previous paragraph for  $^{13}C$  nuclei a different scenario must be considered. Since  $\omega_C$  is smaller than the ESR linewidth, the  $^{13}C$  and the electron dipolar reservoirs are in TM. Within the TM process which governs  $^{13}C$  electron-nucleus relaxation one has  $(1/T_{1C}(T))_{el} = 1/T_{1e}(T)(N_e/N_n)[1 - P_0(T)^2]$ . The ratio  $N_e/N_n$  between the radical and  $^{13}C$  concentrations

<sup>2</sup> One can consider the hyperfine interaction between the protons and the neighbouring radical electron spins in a region comprised between an inner sphere having the radius of the radical  $R_1 = 5.8 \text{ \AA}$ , and an outer sphere with radius  $R_2 = (3 \cdot 0.74/4\pi c)^{1/3} = 26.9 \text{ \AA}$ , corresponding to half of the average distance among the radicals in PA15. In this case, on neglecting the effect of spin diffusion,  $\langle 1/r_{eH}^6 \rangle = 1/(R_1 R_2)^3$ , yields an estimate of the average hyperfine field of  $\sqrt{\langle \Delta h_{eH}^2 \rangle} = (\mu_0/4\pi)\gamma_e \hbar [S(S+1) \langle 1/r_{eH}^6 \rangle]^{1/2} = 8.2 \cdot 10^{-4} \text{ Tesla}$  at the  $^1H$  site.

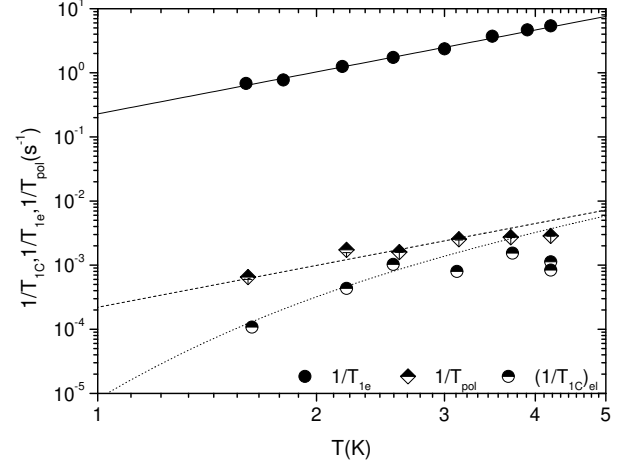


FIG. 11: Comparison among the  $T$  dependence of  $1/T_{1e}$  (black dots),  $1/T_{pol}$  (black and white diamonds) and  $(1/T_{1C})_{el}$  (black and white circles) in PA15 below 4.2 K. The solid line is the fit of  $1/T_{1e}$  according to the power law  $y(T) = aT^b$ , yielding the parameters reported in Tab. I. The dashed line shows the function  $(N_e/N_n)1/T_{1e}$ , while the dotted line gives  $(N_e/N_n)1/T_{1e}[1 - P_0(T)^2]$ .

definitely sets the order of magnitude of  $(1/T_{1C}(T))_{el}$  with respect to  $1/T_{1e}(T)$  and encloses a precise physical meaning: the three body mechanism originating TM, involving two electron spins and one nuclear spin, can flip one of the  $N_n$  nuclear spins, as long as one of the  $N_e$  electrons relaxes to thermal equilibrium. The electron contribution to  $^{13}C$  spin-lattice relaxation  $(1/T_{1C}(T))_{el} = (1/T_{1C}(T))_{PA15} - (1/T_{1C}(T))_{PA}$  derived from the experimental data sets is shown in Fig. 11 (black and white circles). It is remarkable to notice that below 4 K  $(1/T_{1C}(T))_{el}$  data quantitatively follow the trend of the dotted function  $1/T_{1e}(T)(N_e/N_n)[1 - P_0(T)^2]$ , derived from the fit function of the experimental  $1/T_{1e}(T)$  data (Table I), with no adjustable parameter. This is a clear evidence that indeed the  $^{13}C$  spin ensemble and the electron dipolar reservoirs are strongly coupled in the TM, at least for  $T < 4 \text{ K}$ . This important observation is further supported by the  $T$  dependence of  $1/T_{pol}(T)$ , as discussed in the following subsection.

The functional  $T$  dependence  $1/T_{1e} \propto T^{2.2}$  has been ascribed to scattering with the glassy modes, although a sizeable dependence of the  $1/T_{1e}$  magnitude on  $c$  is also expected from previous investigations [15, 16]. Even if literature data on  $1/T_{1e}$  measured in different experimental setup and at different fields are partially contradictory [14–16, 26, 41, 42], both the measurements at 1.2 K shown in [16] and our measurements in the 1.6–4.2 K range at higher  $c$  (unpublished data), consistently evidence a linear dependence  $1/T_{1e} \propto c$  for trityl radicals in PA. Thus, electron spin-lattice relaxation in trityl doped PA can be written as  $1/T_{1e}(T) = (1/T_{1e})_g(T) + \Omega c$ , where



$(1/T_{1e})_g(T)$  is the term linked to the glassy dynamics and  $\Omega$  is a phenomenological weakly  $T$ -dependent parameter. According to [16]  $(1/T_{1e})_{(PA15)}/(1/T_{1e})_g \sim 2 \div 3$  for  $H = 3.35$  Tesla, indicating that for  $c = 15$  mM the contribution due to dipole-dipole interactions among radicals significantly overcomes the one originated by the scattering with the glassy modes and that  $1/T_{1e}(T)$  should weakly depend on the cooling rate, at variance with nuclear  $1/T_1$ .

Overall, from the above considerations a clear scenario emerges. In PA15 the  $1/T_{1H}$  processes show a  $T$  dependence which is uniquely determined by the properties of the glassy matrix. On the other hand, the dominant relaxation mechanism for  $^{13}\text{C}$  rather involves the coupling of the nuclei to the electron dipolar reservoir through TM. Notably, due to the glassy dynamics which characterizes PA, the magnitude of  $T_{1C}$  and  $T_{1H}$  and their  $T$  dependence can possibly vary among samples containing the same radicals admixed to different molecular substrates or among samples prepared, treated and cooled with different methods, which yield to a different glassy dynamics at low  $T$ . The contribution of the glassy modes to the electron spin-lattice relaxation can also justify some variability of  $T_{1e}$  data measured by different groups in different conditions [14–16, 26, 41, 42], even if the dominant electron-electron dipolar relaxation mechanism yields to a  $1/T_{1e}(T)$  which scarcely depends on the cooling rate.

### E. Dynamical nuclear polarization

As shown in Fig. 9 a nearly quadratic  $T$  dependence is found for  $^{13}\text{C}$   $1/T_{\text{pol}}$ , the DNP build up rate. The most recent models describing DNP through TM [19, 22, 23] have shown how the nuclear polarization under MW irradiation can be deeply influenced by several parameters such as  $T_{1e}$ ,  $T_{\text{ISS}}$ , the contact time between the nuclear Zeeman reservoir and the electron dipolar reservoir, as well as by the dissipative spin diffusion among electrons and the degree of saturation by the MW. The behaviour of  $T_{\text{pol}}$  depends on the ratio  $T_{\text{ISS}}/T_{1e}$ . In particular, in presence of nuclear leakage, for  $T_{\text{ISS}}/T_{1e} \sim 1$  (poor contact between electrons and nuclei), polarization levels much lower and  $T_{\text{pol}}$  values longer than those derived here are expected. On the other hand, for  $T_{\text{ISS}}/T_{1e} \ll 1$ , the polarization should increase and  $T_{\text{pol}}$  should shorten and depend on  $T_{1e}$ . Indeed in PA15  $1/T_{\text{pol}}$  has the same  $T^2$  dependence of  $1/T_{1e}$  and its order of magnitude matches quantitatively the functional dependence of  $(N_e/N_N)1/T_{1e}$  below 4 K (dashed curve in Fig. 11). Thus, it is tempting to state that a very efficient contact is actually attained. Remarkably, below 4 K the ratio  $T_{\text{pol}}(T)/T_{1C}(T)_{el}$  behaves as  $[1 - P_0(T)^2]$ . This can happen only if both polarization under MW irradiation and  $T_{1C}$  relaxation proceed through the same TM processes.

Both the polarization and the relaxation time of PA15

are consistent with the TM regime, whereas the experimental  $P_{N\infty}$  (Fig. 10) is substantially smaller than the one predicted by the traditional Borghini model and a mechanism of DNP-dissipation should be identified. The dissipation inside the nuclear reservoir via  $^{13}\text{C}$  spin-lattice relaxation is expected to be irrelevant because the cooling procedure affects the value of  $T_{1C}$  of PA, but not  $P_{N\infty}$  and only weakly  $T_{1e}$ , which mainly depends on  $c$ . Thus the dissipation mechanism does likely affect directly the electron reservoir and can be induced either by a limited microwave power [23, 43] or by the presence of dissipative processes in the spectral diffusion as discussed in [19]. At this stage we cannot exclude one of the two mechanisms, or a combination of the two. Our simulations of the rate equation model introduced in [19, 22, 23] show that the bending behaviour observed in Fig. 10 is consistent with both mechanisms.

Now, the quality of the electron-nucleus contact in PA seemingly evolves on raising  $T$  up to 4 K. In fact, in Fig. 11 a deviation from the dotted and the dashed curves, tracing the good contact trend, is noted around  $T \sim 4$  K for  $1/T_{1C}$  and  $1/T_{\text{pol}}$ . Both time constants become longer than expected, which likely indicates a substantial degradation of the electron-nucleus contact. We possibly ascribe the worsening of the electron-nucleus contact on raising  $T$  to the shortening of  $T_{1e}$ . Infact, for  $T \approx 4$  K,  $T_{1e}$  is around 200 ms, a value close to the effective spin diffusion time [44]  $(N_n/N_e)T_{2C} = 190$  ms, which in turn determines the effective order of magnitude of  $T_{\text{ISS}}$  between the electron dipolar reservoir and the whole nuclear spin ensemble. Then, as explained before, for  $T = 4$  K the threshold of the bad contact regime  $T_{1e} \approx T_{\text{ISS}}$  is matched, the polarization bottleneck becomes  $T_{\text{ISS}}$  and  $T_{1C}$  and  $T_{\text{pol}}$  become longer than expected in the good contact scenario. On the other hand, it should be noted that in the explored  $T$  range any modulation of electron-nucleus coupling by the glassy dynamics looks definitely ineffective. Infact, since in PA15 the modulation of the electron-nucleus distances occurs over the frequency scales of the glassy dynamics,  $10^4 \text{ s} < \langle 1/\tau_c \rangle < 10^5 \text{ s}$ , and considering that the magnitude of the dipolar coupling of the electron spins with the nearby nuclei  $\Delta h$  is such that  $\gamma_{^{13}\text{C}}\Delta h \geq \langle 1/\tau_c \rangle$ , the TM mixing process is marginally affected by that dynamics, in agreement with the absence of any effect of the cooling history on the DNP parameters.

Definitely one can conclude that in PA15 for  $T < 4$  K TM occurs in a good contact regime where  $1/T_{\text{pol}} \propto 1/T_{1e}(T)$ , while for  $T > 4$  K a bad contact regime is attained. The  $T$  dependence of  $P_{N\infty}$  can be explained as well resorting to TM models combined with dissipative mechanisms located in the electron spin system.

## V. CONCLUSIONS

Through a series of nuclear spin-lattice relaxation measurements and DNP experiments, both in pure PA and in

radical doped PA, it was possible to evidence that several microscopic parameters relevant for the understanding of the dynamical nuclear polarization processes follow the same quadratic  $T$  dependence. This trend is interpreted in terms of the glassy dynamics which characterize the PA at low  $T$ . Notably the  $T$  dependence of the DNP build up time, of the electron contribution to  $1/T_{1C}$  and of the saturation polarization are found in agreement with the TM regime with a very good thermal contact between the nuclear and the electron non-Zeeman reservoirs between 1.6 K and 4 K, where  $1/T_{pol} \propto 1/T_{1e}(T)$ . Above 4 K the TM occurs through a less efficient contact, probably due to the shortening of  $T_{1e}$  which becomes of the order of  $T_{ISS}$ . Definitively, this information gives an interesting feedback to the latest theoretical developments, pointing out the relevance of the electron spin relaxation processes, but more specifically claiming a central role for the lattice excitations in determining the ultimate DNP performances.

## VI. APPENDIX

### A. Dependence of the pyruvic acid dynamics on the cooling rate

The dependence of the experimental results on the cooling method was verified by using two different procedures: *a*) a slow pre-cooling inside a bath cryostat from room  $T$  to 150 K at -0.5 K/min, followed by a rapid cooling caused by the liquid helium fill; *b*) a flash freezing of the samples in liquid nitrogen, followed by immersion in liquid helium. Hereafter the first method will be indicated as slow cooling (sc), while the second as fast cooling (fc). Nuclear  $1/T_1$  data showed a different behaviour with respect to the adopted cooling method in both PA and in PA15 (Fig. 12). This variation is likely due to a change in the matrix dynamics properties for different cooling procedures, which is typically observed in glasses. The comparison among  $1/T_{1C}(T)$  in PA and PA15, points out that upon performing a fast cooling  $1/T_{1C}(T)$  doubles in PA, while it only increases by a ratio of 1.5 in PA15. The reason of this difference is ascribed to the additional presence in PA15 of the relaxation term  $(1/T_{1C})_{el}$  due to the thermal mixing with the electrons, which is rather insensitive to the cooling rate, as  $1/T_{pol}(T)$ .

### B. Calculation of $T_{1e}$ from low flip angle acquisitions

As explained, it is possible to quantify  $T_{1e}$  by following the time variation of  $\Delta\omega_0$ . In PA15 the shift can be described by the sum  $\Delta\omega_0 = \Delta M_{IS} + \Delta M_{II}$ , where  $\Delta M_{IS} \propto P_e$  is generated by the hyperfine coupling between the nuclei and the electrons and  $\Delta M_{II} \propto P_N$  by the dipolar nucleus-nucleus interactions [13]. Indeed, since for low  $c$   $\Delta\omega_0$  is small (300 Hz at 1.2 K in PA15 [14, 15])

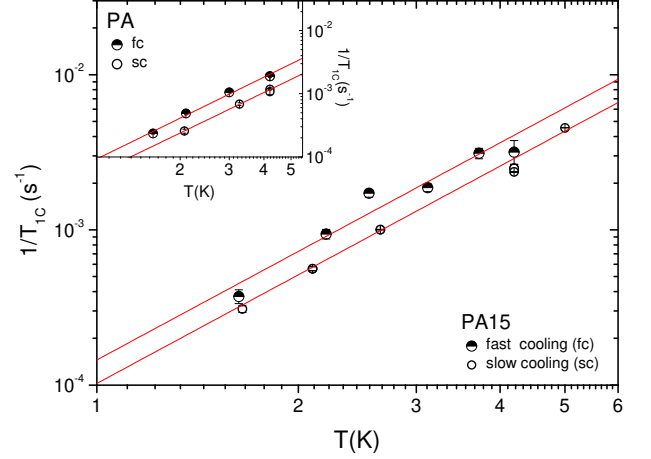


FIG. 12: Log-log plot of  $1/T_{1C}(T)$  measured in PA15 after a slow cooling (white circles) and a fast cooling procedure (black and white circles) below 4.2 K. Inset: Log-log plot of  $1/T_{1C}(T)$  measured in PA after a slow cooling (white circles) and a fast cooling procedure (black and white circles) below 4.2 K. The red lines are fits to the power law  $y(T) = aT^b$ .

its estimate from standard NMR line fits is critical. Conversely, it is rather advantageous to monitor it indirectly by analyzing the oscillations it induces in the NMR signal in the time domain.

When a line shift  $\Delta\omega_0$  from the reference frequency of the NMR spectrometer  $\omega_0$  is present, having moreover the NMR signal envelope  $s(t)$  and an arbitrary phase  $\phi$ , in the domain of time ( $t$ ) the imaginary component of the NMR signal  $Im(t)$  has the form

$$Im(t) = x(t) \sin[(\Delta\omega_0 t) + \phi]. \quad (11)$$

In particular, in the experiment performed to measure  $T_{1e}$ , also  $\Delta\omega_0$  varies with time, but on the time scale of the whole NMR acquisition. The second time variable  $t'$ , triggered to the start of the experiment and with maximum value  $N(\tau + TD)$ , where  $TD$  is the time domain of the single acquisition and  $\tau$  the time delay between acquisitions, describes time evolution  $\Delta\omega_0(t')$ . Then Eq. 11 more properly rules as:

$$Im(t, t') = x(t) \sin[(\Delta\omega_0(t')t) + \phi], \quad (12)$$

and its integral as

$$I(t') = \int_{\tau_1}^{\tau_2} Im(t, t') dt, \quad (13)$$

in which the bounds  $\tau_1$  and  $\tau_2$  should be fixed in the interval in which  $|s(t)|^2 \neq 0$ .

In this work the behaviour of  $I(t')$  in Eq.12 was verified by means of a Python script on considering the complete shift dynamics  $\Delta\omega_0(t') = \Delta M_{II}(t') + \Delta M_{IS}(t')$ .

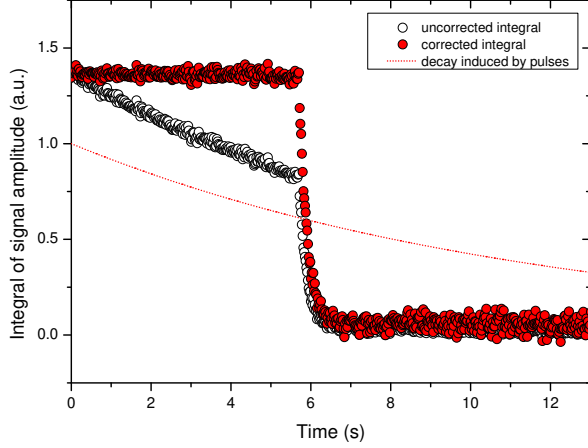


FIG. 13: Simulation of the time dependence of the integral of the imaginary signal  $I(t')$  in the sequence used for the  $T_{1e}$  measurement at 4.2 K. The red dotted line shows the artificial decay induced by the read-pulses, the white circles show the uncorrected  $I(t')$  as obtained by the simulation, the red circles correspond to  $I(t')$  divided by the values of the red dotted line. The curves were simulated by setting  $\Delta M_{IS} = 1$  kHz and  $\Delta M_{IS}/\Delta M_{II} = 10$ .

The NMR signal was modelled to a Gaussian decay, with  $\sigma = 105 \mu\text{s}$  and an initial signal to noise ratio equal to 500. The simulation took into account also the reduction of the signal amplitude operated by the read-out pulses (Fig.13). At time  $\bar{t}'$ , when MW are switched off, for each  $T$   $P_N(\bar{t}')/P_e(\bar{t}')$  was set to the maximum value  $P_{N\infty}(T)/0.5$ , calculated by taking into account that  $P_N(T)(\bar{t}') < P_{N\infty}(T)$  and  $P_e(\bar{t}') \geq 0.5$ , the value of the residual electronic polarization  $P_e^{res}$  expected for saturation at the frequency optimal for DNP [15]. For  $t' > \bar{t}'$  considering both  $T_{1e}$  and  $T_{1N}$  spin-lattice relaxation processes and that  $P_N$  is reduced on increasing  $t'$  by the application of the read out pulses (see Eq. 1), the following laws were assumed to describe nuclear and electronic polarization

$$P_e(t') = (P_e^{res} - P_{E0}) \exp(-t'/T_{1e}) + P_{E0} \quad (14)$$

$$P_N(t') = (P_N(\bar{t}') - P_{N0}) \exp \left[ -t' \left( \frac{1}{T_{1N}} - \frac{\ln(\cos \alpha)}{\tau} \right) \right] + P_{N0}, \quad (15)$$

where  $P_{N0}$  and  $P_{E0}$  are the thermal equilibrium values for nuclear and electronic polarization respectively. In Eq. 15  $T_{1N}$  assumed the experimental values in Fig.5,  $\alpha = 3^\circ$  and  $\tau$  ranged from 15 ms at 4.2 K to 100 ms at 1.8 K. Remarkably,  $P_N(t')$  has an effective relaxation rate which is driven mainly by the term  $\exp(t' \ln(\cos \alpha)/\tau)$ , since  $1/T_{1N} \ll \ln(\cos \alpha)/\tau$ , and is increased sensibly by fast repetition (12 s for  $\tau = 19$  ms). Eq. 14 and 15 were used to calculate  $\Delta\omega_0(t')$  and then  $I(t')$ . As expected, in spite of an increase of  $P_N(\bar{t}')/P_e(\bar{t}') \simeq 0.26$  at 1.8 K, the

simulation showed that imposing  $T_{1e} \simeq 1$  s,  $T_{1N} \simeq 1800$  s and  $\tau = 100$  ms,  $I(t')$  is perfectly fit to a simple exponential decay until 60 s after  $\bar{t}'$  with a decay constant of 1 s. At  $T=4.2$  K for  $T_{1e} \simeq 0.2$  s,  $T_{1N} \simeq 400$  s,  $\tau = 19$  ms, until 12 s after  $\bar{t}'$  the simple exponential fit of  $I(t')$  led to a decay constant of 0.22 s, +11 % with respect to the initial simulation parameter, only when increasing  $P_N(\bar{t}')/P_e(\bar{t}')$  to 0.5, equal to 5 times the maximum reachable value at this T. Finally, the results didn't depend on the integration interval chosen to calculate  $I(t')$ .

$I(t')$  obtained by the experiment was divided by the expression in Eq 1, yielding a curve properly detrended by the artificial decay induced by pulses (Fig.3). Eq. 1 was considered valid also for  $t' < \bar{t}'$  since for  $\tau \ll T_{pol}$  the build up, occurring on times of the order of  $T_{pol} \simeq 400$  s  $\div$  1200 s is overwhelmed by the fast repetition of the read out pulses. Accordingly for all Ts and  $t' > \bar{t}'$ , experimental data of  $I(t')$  were suitably fit to a single exponential decay, after performing a smoothing procedure consisting in the unweighted averaging of 3 adjacent data points.

### C. Calculation of the $T_{1C}(T)/T_{1H}(T)$ ratio starting from model nuclear interactions

In the following we are going to consider the contributions to spin-lattice relaxation of  $1\text{-}^{13}\text{C}$  and  $^1\text{H}$  deriving from nuclear dipole-dipole interactions, CSA and hyperfine dipolar interactions.

The spin-lattice relaxation in case of homonuclear dipolar interactions between spins I will be described by [39]

$$\left(\frac{1}{T_1}\right)_{I-I} = \frac{2}{5} \left(\frac{\mu_0}{4\pi}\right)^2 \gamma_I^4 \hbar^2 I(I+1) \left\langle \frac{1}{r_{II}^6} \right\rangle [J(\omega_I) + 4J(2\omega_I)], \quad (16)$$

where  $\gamma_I$  is gyromagnetic ratio of spins I,  $\langle 1/r_{II}^6 \rangle$  indicates the average of the inverse sixth power of I-I distances and  $J(\omega_I)$  the spectral density at the Larmor frequency  $\omega_I = \gamma_I H$  of spins I. The spin-lattice relaxation of spins I in case of interactions between spins I and S will be described by

$$\left(\frac{1}{T_1}\right)_{S-I} = \frac{2}{15} \left(\frac{\mu_0}{4\pi}\right)^2 \gamma_I^2 \gamma_S^2 \hbar^2 S(S+1) \left\langle \frac{1}{r_{SI}^6} \right\rangle \times [J(\omega_I - \omega_S) + 3J(\omega_I) + 6J(\omega_I + \omega_S)], \quad (17)$$

where  $\gamma_S$  is gyromagnetic ratio of spins S,  $\langle 1/r_{SI}^6 \rangle$  is the average of the inverse sixth power of S-I distances and  $\omega_S = \gamma_S H$  the Larmor frequency of spins S. Finally spin-lattice relaxation due to CSA at the  $1\text{-}^{13}\text{C}$  site will be expressed as [40]

$$\left(\frac{1}{T_1}\right)_{CSA} = \frac{2}{15} \omega_C^2 \Delta\sigma^2 J(\omega_C), \quad (18)$$

where  $\Delta\sigma$  is the CSA tensor anisotropy.

In the following all the quantities referring to generic spins I and S will be specialized to the case of protons

(using subscript H), carbons (subscript C) and electrons (subscript e). For homonuclear interactions among protons the mean square amplitude of the fluctuation frequencies of the dipolar field  $\langle\Delta\omega_{\perp HH}^2\rangle$  inducing the spin lattice relaxation is related to the powder line second moment  $\langle\Delta\omega_{HH}^2\rangle$  to the relation

$$\langle\Delta\omega_{\perp HH}^2\rangle = \frac{2}{5} \left(\frac{\mu_0}{4\pi}\right)^2 \gamma_H^4 \hbar^2 I(I+1) \left\langle \frac{1}{r_{HH}^6} \right\rangle = \frac{2}{3} \langle\Delta\omega_{HH}^2\rangle, \quad (19)$$

with spin I of protons equal to 1/2, while for heteronuclear interactions the formula becomes

$$\langle\Delta\omega_{\perp HC}^2\rangle = \frac{2}{15} \left(\frac{\mu_0}{4\pi}\right)^2 \gamma_H^2 \gamma_C^2 \hbar^2 S(S+1) \left\langle \frac{1}{r_{HC}^6} \right\rangle = \frac{1}{2} \langle\Delta\omega_{HC}^2\rangle, \quad (20)$$

with spin S of carbons equal to 1/2.

The important assumptions we make are:

1.  $J(\omega)$  is the same for all the relaxation contributions and is the one related to the lattice dynamics.
2.  $J(\omega)$  is approximated to the slow motion regime form considering an average correlation frequency, yielding  $J(\omega_L) \simeq \frac{1}{\omega_L}^2 \langle \frac{1}{\tau_c} \rangle$
3. The amplitude of the local fluctuating fields probed by the nuclei is the one estimated from the linewidth analysis of 1- $^{13}\text{C}$  and  $^1\text{H}$ .

From the literature data [16] it is possible to extract  $\langle\Delta\omega_{HC}^2\rangle = \langle\Delta\omega^2\rangle - \langle\Delta\omega_{CSA}^2\rangle = 465 \text{ (krad/s)}^2$ , considering the total carbon Full Width at Half Maximum (FWHM) of  $(5.9)^2 * 4\pi^2 \text{ (krad/s)}^2$ , the broadening due to CSA  $(4.8)^2 * 4\pi^2 \text{ (krad/s)}^2$  and neglecting carbon-carbon interactions. Then  $\langle\Delta\omega_{\perp HC}^2\rangle = 232.5 \text{ (krad/s)}^2$ . From the proton line one obtains  $\langle\Delta\omega_{HH}^2\rangle = \langle\Delta\omega^2\rangle - \langle\Delta\omega_{HC}^2\rangle = 35066 \text{ (krad/s)}^2$  and thus  $\langle\Delta\omega_{\perp HH}^2\rangle = 23377 \text{ (krad/s)}^2$ .

The average hyperfine field probed by the nuclei can be calculated inside a sphere centred on the radical (see Subsection 4.3). The calculation yields the result of  $8.2 \cdot 10^{-4}$  Tesla for both nuclei assuming the same electron-nucleus distance, thus for protons  $\langle\Delta\omega_{\perp eH}^2\rangle = 2/5 (\mu_0/4\pi)^2 \gamma_H^2 \gamma_e^2 \hbar^2 S(S+1) \langle 1/r_{eH}^6 \rangle = 19172 \text{ (krad/s)}^2$  and for carbons  $\langle\Delta\omega_{\perp eC}^2\rangle = 2/5 (\mu_0/4\pi)^2 \gamma_C^2 \gamma_e^2 \hbar^2 S(S+1) \langle 1/r_{eC}^6 \rangle = 1198 \text{ (krad/s)}^2$ .

For the calculation of  $1/T_{1H}$  at 0.87 Tesla  $\omega_H/2\pi = 37.02 \text{ MHz}$  and  $\omega_C \simeq 1/4\omega_H$ . For the calculation of  $1/T_{1C}$  at 3.46 Tesla  $\omega_C/2\pi = 37.02 \text{ MHz}$  and  $\omega_H \simeq 4\omega_C$ . The ratio  $T_{1C}(T)/T_{1H}(T)$  is then estimated taking into account the experimental condition  $\omega_L = \omega_H = \omega_C$ . For PA, starting from the model of Eq. 2 and 4 and considering  $\langle\Delta\omega_{CH}^2\rangle = \langle\Delta\omega_{HC}^2\rangle$  in the slow motion regime the ratio reduces to

$$\begin{aligned} \frac{1/T_{1H}}{1/T_{1C}} &= 2 \frac{\langle\Delta\omega_{\perp HH}^2\rangle}{(\frac{1}{9} + 3 + \frac{6}{25})\langle\Delta\omega_{\perp HC}^2\rangle + \frac{2}{15}\omega_L^2\Delta\sigma^2} + \\ &+ \frac{(\frac{1}{9} + 3 + \frac{96}{25})\langle\Delta\omega_{\perp HC}^2\rangle}{(\frac{1}{9} + 3 + \frac{6}{25})\langle\Delta\omega_{\perp HC}^2\rangle + \frac{2}{15}\omega_L^2\Delta\sigma^2} = \\ &= 54. \end{aligned} \quad (21)$$

The calculation retrieves a value very close to the average  $T_{1C}(T)/T_{1H}(T) \simeq 53$  estimated from the experimental data for  $T < 4.2 \text{ K}$ , confirming that  $1/T_1$  models in Eq. 2 for  $^1\text{H}$  and in Eq. 4 for  $^{13}\text{C}$  are correct.

In the doped sample PA15 it is necessary to introduce also the hyperfine contribution to both 1- $^{13}\text{C}$  and  $^1\text{H}$  relaxation. On taking into account the hyperfine dipolar interactions one has

$$\begin{aligned} \frac{1/T_{1H}}{1/T_{1C}} &= 2 \frac{\langle\Delta\omega_{\perp HH}^2\rangle}{(\frac{1}{9} + 3 + \frac{6}{25})\langle\Delta\omega_{\perp HC}^2\rangle + \frac{2}{15}\omega_L^2\Delta\sigma^2 + \langle\Delta\omega_{\perp eC}^2\rangle} + \\ &+ \frac{(\frac{1}{9} + 3 + \frac{96}{25})\langle\Delta\omega_{\perp HC}^2\rangle}{(\frac{1}{9} + 3 + \frac{6}{25})\langle\Delta\omega_{\perp HC}^2\rangle + \frac{2}{15}\omega_L^2\Delta\sigma^2 + \langle\Delta\omega_{\perp eH}^2\rangle} + \\ &+ \frac{\langle\Delta\omega_{\perp eH}^2\rangle}{(\frac{1}{9} + 3 + \frac{6}{25})\langle\Delta\omega_{\perp HC}^2\rangle + \frac{2}{15}\omega_L^2\Delta\sigma^2 + \langle\Delta\omega_{\perp eC}^2\rangle} = \\ &= 32. \end{aligned} \quad (22)$$

The measurement of  $^1\text{H}$  has been performed in the non labelled sample uPA, so the theoretical prediction should neglect the proton-carbon interactions for  $^1\text{H}$ , definitely giving  $T_{1C}(T)/T_{1H}(T) = 31$ . Thus upon considering the contribution to proton and carbon relaxation associated to the lattice dynamics, one finds a theoretical value close to  $T_{1C}(T)/T_{1H}(T) \simeq 28 \pm 3$ , derived from the experimental data measured below 4.2 K in PA15. In absence of other experimental evidences, this could suggest that the relaxation rates can be explained by drawing upon this mechanism alone. However this results should be better regarded as an alternative explanation based on rough estimates of the fluctuating local fields and on the naive assumption of a common  $\tau_c$  for all the processes. In particular, one should be aware that the calculation of the dipolar field produced by the electrons on the nuclei does not take into account the effect of nuclear spin diffusion (see Section 4.3). On the other hand, the behaviour of  $(1/T_{1C})_{el}$  as a function of T (Fig. 11) is rather suitably reproduced by a TM model which does not imply the introduction of any tunable parameter and which is able to account for the polarization build up rates, thus providing a cleaner interpretation scheme for the electron contribution to the  $^{13}\text{C}$  nuclear relaxation. Moreover, a sizeable contribution to spin-lattice relaxation due to TM must be invoked also to explain a dependence of  $(1/T_{1C}(T))$  on the cooling rate sensibly weaker in PA15 than in PA (see Appendix 6.1). If in PA15  $(1/T_{1C}(T))_{el}$  contained spectral density terms only connected to the glassy dynamics, one would rather have expected the same variation of  $(1/T_{1C}(T))$  with the cooling rate in both samples.

## Acknowledgements

We gratefully acknowledge A. Rigamonti for fruitful discussions and Albeda Research for their contributions



to DNP sample preparation. This study has been supported in part by the COST Action TD1103 (European Network for Hyperpolarization Physics and Methodology in NMR and MRI) and by Regione Piemonte (Misura II.3 del Piano Straordinario per l' Occupazione). More-

over this work has been supported by a public grant from the "Laboratoire d'Excellence Physics Atom Light Mater" (LabEx PALM) overseen by the French National Research Agency (ANR) as part of the "Investissements d'Avenir" program (reference: ANR-10-LABX-0039).

- 
- [1] A. J. Rossini, A. Zagdoun, M. Lelli, A. Lesage, C. Copret, and L. Emsley, *Accounts of Chemical Research* **46**, 1942 (2013), pMID: 23517009, <http://dx.doi.org/10.1021/ar300322x>, URL <http://dx.doi.org/10.1021/ar300322x>.
  - [2] A. B. Barnes, G. De Paepe, P. C. A. van der Wel, K.-N. Hu, C.-G. Joo, V. S. Bajaj, M. L. Mak-Jurkauskas, J. R. Sirigiri, J. Herzfeld, R. J. Temkin, et al., *Applied Magnetic Resonance* **34**, 237 (2008), ISSN 0937-9347, URL <http://dx.doi.org/10.1007/s00723-008-0129-1>.
  - [3] Q. Z. Ni, E. Daviso, T. V. Can, E. Markhasin, S. K. Jawa, T. M. Swager, R. J. Temkin, J. Herzfeld, and R. G. Griffin, *Accounts of Chemical Research* **46**, 1933 (2013), pMID: 23597038, <http://dx.doi.org/10.1021/ar300348n>, URL <http://dx.doi.org/10.1021/ar300348n>.
  - [4] P. Dutta, G. V. Martinez, and R. J. Gillies, *Biophys. Rev.* **5**, 271 (2013).
  - [5] J. H. Ardenkjaer-Larsen, B. Fridlund, A. Gram, G. Hansson, L. Hansson, M. H. Lerche, R. Servin, M. Thaning, and K. Golman, *PNAS* **100**, 10158 (2003).
  - [6] J. Wolber, F. Ellner, B. Fridlund, A. Gram, H. Jóhannesson, G. Hansson, L. Hansson, M. Lerche, S. Mnsson, R. Servin, et al., *Nuclear Instruments and Methods in Physics Research Section A: Accelerators, Spectrometers, Detectors and Associated Equipment* **526**, 173 (2004).
  - [7] A. Comment, B. van den Brandt, K. Uffmann, F. Kurdzesau, S. Jannin, J. Konter, P. Hautle, W. Wenckebach, R. Gruetter, and J. van der Klink, *Concepts in Magnetic Resonance Part B: Magnetic Resonance Engineering* **31B**, 255 (2007).
  - [8] K. Golman, R. in't Zandt, and M. Thaning, *PNAS* **103**, 11270 (2006).
  - [9] K. Golman, R. in't Zandt, M. Lerche, R. Pehrson, and J. H. Ardenkjaer-Larsen, *Cancer Res.* **66**, 10855 (2006).
  - [10] J. Kurhanewicz, D. B. Vigneron, K. Brindle, E. Y. Chekmenev, A. Comment, C. H. Cunningham, R. J. DeBerardinis, G. G. Green, M. O. Leach, S. S. Rajan, et al., *Neoplasia* **13**, 81 (2011).
  - [11] G. Lin and Y.-L. Chung, *Biomed Res Int.* **2014**, 625095 (2014).
  - [12] O. J. Rider and D. J. Tyler, *J Cardiovasc Magn Reson.* **15**, 93 (2013).
  - [13] A. Abragam and M. Goldman, *Nuclear order and disorder* (Clarendon Press, Oxford, 1982).
  - [14] J. H. Ardenkjaer-Larsen, S. Macholl, and H. Jóhannesson, *Appl. Magn. Res.* **34**, 509 (2008).
  - [15] H. Jóhannesson, S. Macholl, and J. H. Ardenkjaer-Larsen, *J. Magn. Res.* **197**, 167 (2009).
  - [16] S. Macholl, H. Jóhannesson, and J. H. Ardenkjaer-Larsen, *Phys. Chem. Chem. Phys.* **12**, 5804 (2010).
  - [17] L. Lumata, M. E. Merritt, C. R. Malloy, A. D. Sherry, and Z. Kovacs, *J. Phys. Chem. A* **116**, 5129 (2012).
  - [18] L. Lumata, Z. Kovacs, C. Malloy, A. D. Sherry, and M. Merritt, *Phys. Med. Biol.* **56**, N85 (2011).
  - [19] S. Colombo Serra, M. Filibian, P. Carretta, A. Rosso, and F. Tedoldi, *Phys. Chem. Chem. Phys.* **16**, 753 (2014).
  - [20] L. Lumata, M. E. Merritt, and Z. Kovacs, *Phys. Chem. Chem. Phys.* **15**, 7032 (2013).
  - [21] W. Meyer, J. Heckmann, C. Hess, E. Radtke, G. Reicherz, L. Triebwasser, and L. Wang, *Nuclear Instruments and Methods in Physics Research Section A: Accelerators, Spectrometers, Detectors and Associated Equipment* **631**, 1 (2011).
  - [22] S. Colombo Serra, A. Rosso, and F. Tedoldi, *Phys. Chem. Chem. Phys.* **14**, 13299 (2012).
  - [23] S. Colombo Serra, A. Rosso, and F. Tedoldi, *Phys. Chem. Chem. Phys.* pp. 8416–8428 (2013).
  - [24] T.-C. Ong, M. L. Mak-Jurkauskas, J. J. Walsh, V. K. Michaelis, B. Corzilius, A. A. Smith, A. M. Clausen, J. C. Cheetham, T. M. Swager, and R. G. Griffin, *The Journal of Physical Chemistry B* **117**, 3040 (2013), pMID: 23421391, <http://dx.doi.org/10.1021/jp311237d>, URL <http://dx.doi.org/10.1021/jp311237d>.
  - [25] G. Pages and P. W. Kuchel, *Magnetic Resonance Insights* **6** (2013).
  - [26] S. A. Walker, D. T. Edwards, T. A. Siaw, B. D. Armstrong, and S. Han, *Phys. Chem. Chem. Phys.* **15**, 15106 (2013).
  - [27] D. Shimon, Y. Hovav, A. Feintuch, D. Goldfarb, and S. Vega, *Phys. Chem. Chem. Phys.* pp. 5729–5743 (2012).
  - [28] D. G. Daphna Shimon, Akiva Feintuch and S. Vega, *Phys. Chem. Chem. Phys.* **14**, 5729 (2012).
  - [29] S. Jannin, A. Comment, F. Kurdzesau, J. A. Konter, P. Hautle, B. van den Brandt, and J. J. van der Klink, *J. Chem. Phys.* **128**, 241102 (2008).
  - [30] F. Kurdzesau, B. van den Brandt, A. Comment, P. Hautle, S. Jannin, J. J. van der Klink, and J. A. Konter, *J. Phys. D: Appl. Phys.* **41**, 155506 (2008).
  - [31] M. Plückthun, C. Bradtke, H. Dutz, R. Gehring, S. Goertz, J. Harmsen, P. Kingsberry, W. Meyer, and G. Reicherz, *Nuclear Instruments & Methods in Physics Research Section A-accelerators Spectrometers Detectors and Associated Equipment* **400**, 133 (1997).
  - [32] M. Borghini, *Phys. Rev. Lett.* **20**, 419 (1968).
  - [33] I. D. Reva, S. G. Stepanian, L. Adamowicz, and R. Fausto, *J. Phys. Chem. A* **105**, 4773 (2001).
  - [34] R. Böhmer, G. Diezemann, G. Hinze, and E. Rössler, *Prog. Nucl. Magn. Reson. Spectrosc.* **39**, 191 (2001).
  - [35] J. Wiedersich, N. V. Surovtsev, and E. Rössler, *J. Chem. Phys.* **113**, 1143 (2000).
  - [36] S. Estalji, O. Kanert, J. Steinert, H. Jain, and K. Ngai, *Phys. Rev. B* **43**, 7481 (1991).
  - [37] S. K. Misra, *Spectrochimica Acta Part A* **54**, 22572267 (1998).
  - [38] D. Merunka, M. Kveder, and B. Rakvin, *Chem. Phys. Lett.* **515**, 19 (2011).
  - [39] A. Abragam, *Principles of Nuclear Magnetism* (Oxford

- University Press, 1983).
- [40] J. Kowalewski and L. Maler, *Nuclear Spin Relaxation in Liquids: Theory, Experiments, and Applications* (CRC Press, 2006).
- [41] M. E. M. Lloyd Lumata and Z. Kovacs, *Physical Chemistry Chemical Physics* **15**, 9800 (2013).
- [42] C. Hess, J. Herick, A. Berlin, W. Meyer, and G. Reichers, *Nucl. Instrum. Methods Phys. Res., Sect. A* pp. 69–77 (2012).
- [43] S. Jannin, A. Comment, and J. J. van den Klink, *Appl. Magn. Res.* **43**, 59 (2012).
- [44] W. E. Blumberg, *Physical Review* **119**, 79 (1960).